# Structure optimization of a uni-traveling-carrier photodiode with introduction of a hydro-dynamic model*

Li Guoyu(李国余)[1,†], Zhang Yejin(张冶金)[2], Li Xiaojian(李小健)[1], and Tian Lilin(田立林)[1]

*(1 Institute of Microelectronics, Tsinghua University, Beijing 100084, China)*
*(2 Institute of Semiconductors, Chinese Academy of Sciences, Beijing 100083, China)*

**Abstract:** Characteristics of a uni-traveling-carrier photodiode (UTC-PD) are investigated. A hydro-dynamic model is introduced which takes into account the electrons' velocity overshoot in the depletion region, which is a more accurate high speed device than using the normal drift–diffuse model. Based on previous results, two modified UTC-PDs are presented, and an optimized device is obtained, the bandwidth of which is more than twice that of the original.

**Key words:** UTC-PD; hydro dynamic model; linear doping; linear band-gap
**DOI:** 10.1088/1674-4926/31/10/104005 **PACC:** 4283 **EEACC:** 1475

## 1. Introduction

With the fast development of fiber-optic communication, higher performance of photodiodes (PDs), such as responsibility and bandwidth, is required. For the conventional pin PD, the response speed is at some degree slow[1], and it cannot match the high bandwidth requirement any longer. To overcome the limitation of pin PDs, NTT System Electronics Laboratories has developed a new kind of PD called the uni-traveling-carrier photodiode (UTC-PD)[1] . This kind of PD uses electron as the only active carrier, whose mobility is much larger than that of the hole, so the speed of the device is clearly enhanced. Due to the advantage above, many UTC-PDs have been fabricated since its appearance[2−4], and the performance of real devices is improved by many advanced methods in real processes. In Ref. [5], the bandwidth achieved was as high as 310 GHz. Shi *et al.*[6] proposed a near-ballistic UTC-PD (NBUTC-PD). The saturation current bandwidth product achieved 2952 mA·GHz (120 GHz, 24.6 mA) under 25 Ω loading at V-band. On the other hand, in the simulation field, Banik *et al.*[7] did some research on an optimization method, but the work only focused on the output power optimization and didn't give any results on the bandwidth optimization. Rahman *et al.*[8] gave a somewhat comprehensive statement on the device behavior. However, the work didn't include a detailed study on the optimization methods. Due to the lack of simulation work which provides theoretical analysis and optimization methods, it is necessary to make an overall simulation so as to give a more comprehensive result for the device and help to fabricate higher performance devices.

In this paper, the hydro dynamic (HD) model is utilized to analyze the device performance, and the main contributions of this work are as follows: two modified structures are proposed based on the characteristics of the UTC-PD, and the device is optimized, with the bandwidth improved more than twice that of the original one.

## 2. Device model

A typical structure and the band diagram of the UTC-PD are shown in Fig. 1, and an epitaxial layer structure is presented in Table 1[9] (normal device). The UTC-PD is composed of a neutral narrow-gap absorption layer with high p-type doping and an $n^-$ wide-gap collection layer. A high n-type doping layer called the cliff layer can modulate the electric field in the device, so the performance of the device is enhanced.

This work uses the HD model, and the current densities are expressed as follows[11, 12]:

$$J_n = q\mu_n(n\nabla E_c + k_B T_n \nabla n/q - 1.5nk_B T_n \nabla \ln m_e/q), \quad (1)$$

$$J_p = q\mu_p(p\nabla E_c + k_B T_p \nabla n/q - 1.5pk_B T_p \nabla \ln m_h/q), \quad (2)$$

where the first and second terms are what the DD model only

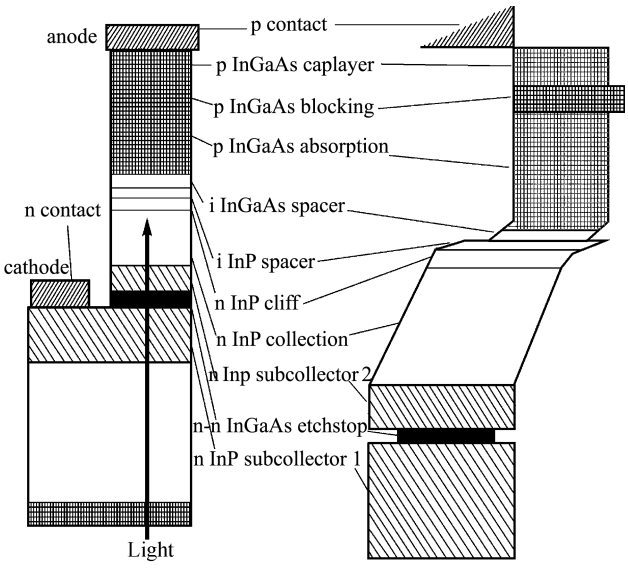


Fig. 1. Typical structure and the band diagram of UTC-PD[10].

* Project supported by the National Natural Science Foundation of China (No. 60736002) and the National High Technology Research and Development Program of China (No. 2007AA03Z408).
† Corresponding author. Email: ligy08@mails.tsinghua.edu.cn
Received 7 January 2010, revised manuscript received 2 May 2010

Table 2. Parameters used in this simulation.

| | InGaAs ($N_A = 1 \times 10^{18}$ cm$^{-3}$) | InP ($N_D = 1 \times 10^{16}$ cm$^{-3}$) |
|---|---|---|
| $\mu_e$ (cm$^2$/(V·s)) | 3500 | 570 |
| $\tau_w$ (ps) | 1 | 1 |
| $\tau_e$ (ps) | 120 | N/A |
| $D_e$ (cm$^2$/s) | 91 | 14.8 |
| $\alpha_{@1.55\mu m}$ (cm$^{-1}$) | 7000 | $\approx 0$ |

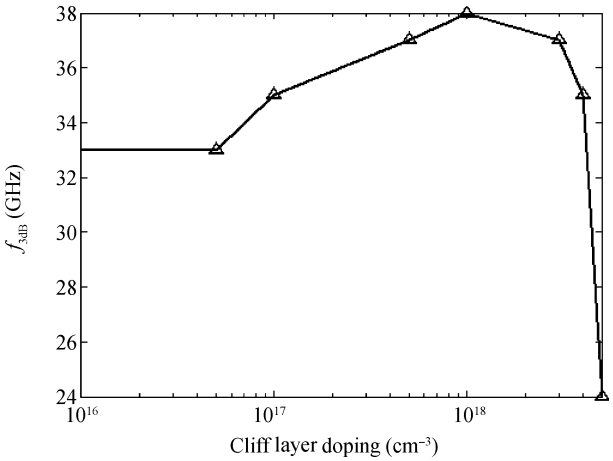


Fig. 2. $f_{3dB}$ versus the cliff layer doping.

Table 1. Epitaxial layer structure for UTC-PD reported in Ref. [9].

| Layer | Thickness (nm) | Doping (cm$^{-3}$) | Band-gap (eV) |
|---|---|---|---|
| p$^{++}$ InGaAs contact | 50 | $3\times10^{19}$ | 0.76 |
| p$^{++}$ InGaAsP blocking | 20 | $2\times10^{19}$ | 0.89 |
| p$^{+}$ InGaAs absorption | 220 | $1\times10^{18}$ | 0.76 |
| InGaAs spacer | 8 | $1\times10^{15}$ | 0.76 |
| InGaAsP spacer | 16 | $1\times10^{15}$ | 1.0 |
| InP spacer | 6 | $1\times10^{15}$ | 1.35 |
| n$^{+}$ InP cliff | 7 | $1\times10^{18}$ | 1.35 |
| n$^{-}$ InP collection | 263 | $1\times10^{16}$ | 1.35 |
| n$^{+}$ InP subcollector | 50 | $5\times10^{18}$ | 1.35 |
| n$^{+}$ InGaAs contact | 10 | $1\times10^{19}$ | 0.76 |

includes. $T_n$ and $T_p$ are the electron and hole temperatures, indicating that the HD model takes the temperature difference between the carrier and lattice into account, due to which the carrier and the lattice will exchange energy within an energy relaxation time. Because the energy relaxation time is usually not equal to the momentum relaxation time, a so-called overshoot phenomenon happens and improves the device frequency response.

## 3. Characteristics and analysis

In the simulation, the Taurus[13] CAD tool is used to solve the required equations, with a bottom illumination at 1.55 $\mu$m wavelength and a 2 V reverse bias. The device area is 25 $\mu$m$^2$ and the load resistance is 50 Ω. All the experiments are based on the normal device. The characteristics of UTC-PD are completely analyzed and validated with the results in Ref. [9] for verification, which demonstrates that our simulation can achieve a good agreement with the results in Ref. [9]. The parameters used in our simulation are presented in Table 2[8, 13].

The bandwidth decreases significantly with the growth in absorption layer thickness ($W_A$), so the bandwidth can be improved by decreasing $W_A$, but it cannot be too small to ensure the output current of the device. But when the collection layer thickness ($W_C$) increases, the bandwidth also increases. The velocity in the spacer and collection regions is very high and the transit time in these regions is relatively short compared to the RC time constant. Therefore, when the collection layer thickness increases, the effective capacitance decreases as well as the RC time constant, and the bandwidth gets larger.

The bandwidth decreases as the absorption layer doping increases. The electron mobility goes down as the doping concentration rises[14], so does the diffusion coefficient according to the Einstein relation. And it will take a longer time to transit through the absorption region. As a result, the bandwidth goes down. And it has the same trend with the collection layer doping. As the doping increases, the collection layer can't be totally depleted. So the remaining electrons prevent the drift of electrons from transiting through the collection layer. As a result, the transit time increases and the bandwidth decreases.

The relationship between the bandwidth and the cliff layer doping is shown in Fig. 2. As is shown, the bandwidth increases from 33 to 38 GHz as the cliff layer doping grows from $1 \times 10^{16}$ to $1 \times 10^{18}$ cm$^{-3}$, and decreases to 24 GHz at $5 \times 10^{18}$ cm$^{-3}$. The reason for this is that the cliff layer can modulate the electric field in the device, and when the doping is about $1 \times 10^{18}$ cm$^{-3}$, the electric field in both the spacer layer and the collection layer reaches the intensity that makes the electron velocity very high, bringing a peak bandwidth for the device. Due to the fact that the overshoot velocity is greatly related to the electric field, the cliff layer doping should be carefully determined for the device.

## 4. Modified and optimization structures

For normal UTC-PDs, the electric field in the absorption region is very small since it is highly doped, where the motion is mainly diffused due to the electron concentration gradient. Because the diffusion process is much slower than the drift one, it significantly affects the bandwidth. We consider introducing an electric field[8] in the absorption region to address this problem.

### 4.1. Linear doping in the absorption region

We created a modified structure with the absorption region p$^{+}$ linearly doped from $2 \times 10^{18}$ cm$^{-3}$ near the barrier region to $5 \times 10^{17}$ cm$^{-3}$ adjacent to the spacer region. The field distribution in the absorption region of this modified device is shown

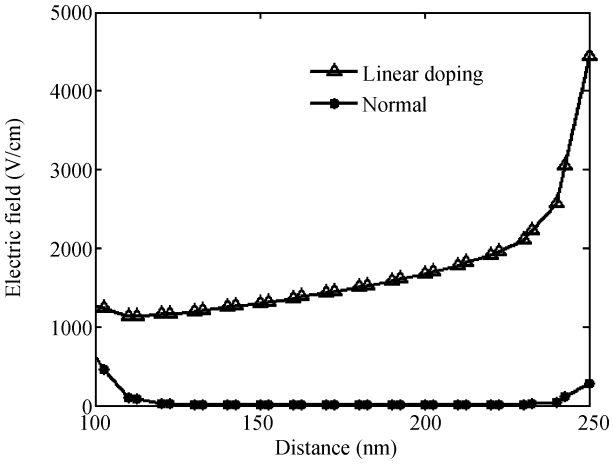


Fig. 3. Electronic field in the absorption region with the collection layer doping $1 \times 10^{16}$ cm$^{-3}$.

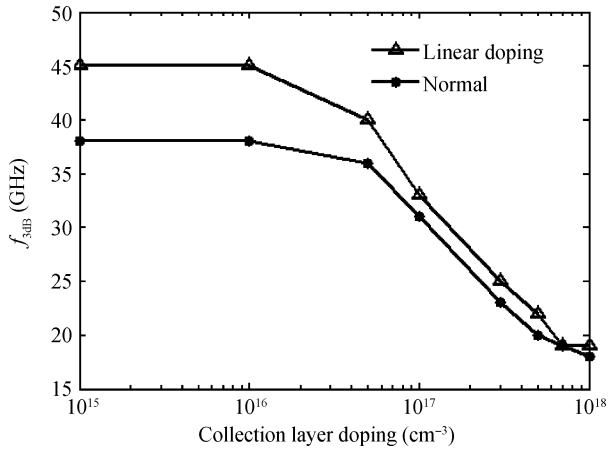


Fig. 4. $f_{3dB}$ versus the collection layer doping.

in Fig. 3, which shows that the electric field is much larger than that of the device in Table 1. It is shown in Fig. 4 that for the modified device, the bandwidth is 45 GHz when the collection layer doping is $1 \times 10^{16}$ cm$^{-3}$, and for the normal device it is only 38 GHz.

### 4.2. Linear energy-band in the absorption region

We also designed a modified structure, with the band-gap in the absorption region linearly from 0.76 to 0.69 eV by using linear composition of InGaAs. The behavior of this device is similar to that of the linearly doped one proposed above, and the artificial electric field is about 500 V/cm (Fig. 5). It can be seen from Fig. 6 that the bandwidth of this device is 47 GHz, which is 9 GHz larger than that of the normal one at $W_C = 263$ nm, so the bandwidth can also be improved by this method.

### 4.3. Optimization

From the proposed modification methods above, another structure is considered by combining the linear doping, and composition together, that is, the absorption region $p^+$ linearly doped from $2 \times 10^{18}$ cm$^{-3}$ near the barrier region to $5 \times 10^{17}$ cm$^{-3}$ adjacent to the spacer region and the band-gap in the absorption region linearly from 0.76 to 0.69 eV, to increase the electronic field in the absorption region. The electronic field

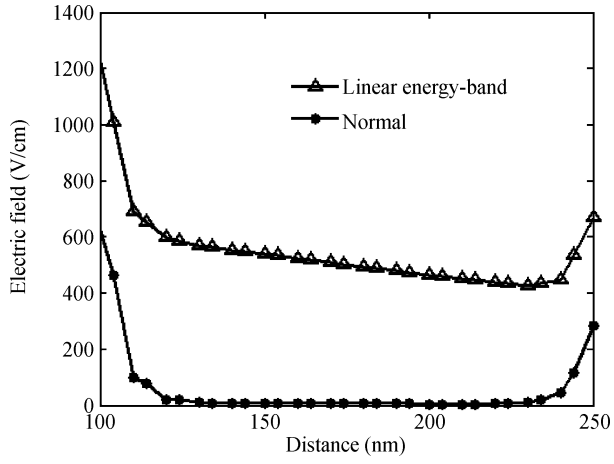


Fig. 5. Electronic field in the absorption region with versus the collection layer thickness.

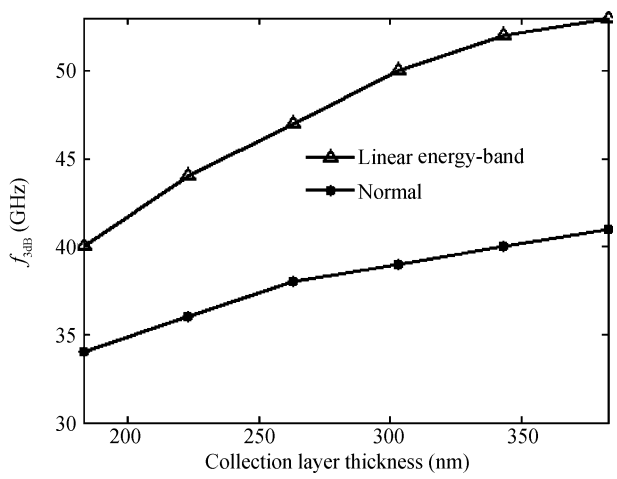


Fig. 6. $f_{3dB}$ the collection layer thickness at 263 nm.

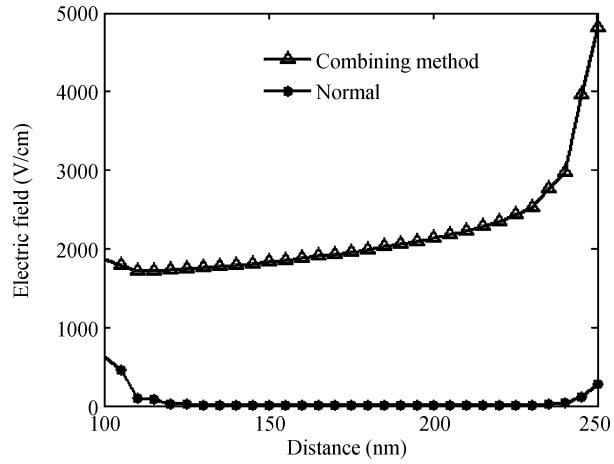


Fig. 7. Electronic field in the absorption region with the collection layer thickness at 263 nm.

distribution in the absorption region is shown in Fig. 7 and the performance of the bandwidth is presented in Fig. 8. For comparison, the performance of the bandwidth of the structure in Table 1 is added. It shows that the bandwidth increases from

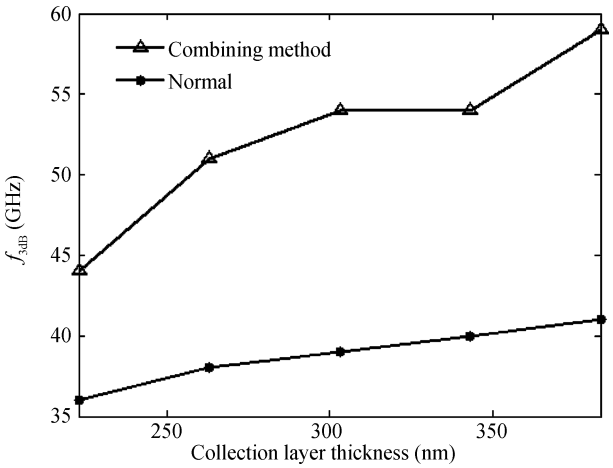


Fig. 8. $f_{3dB}$ versus the collection layer thickness.

38 to 51 GHz, nearly by 30%.

Finally, an optimized structure is obtained by using this method. The parameters are based on the structure, as shown in Table 1. As an optimization condition, the smallest response efficiency is set to 0.1 A/W and the minimal value of $W_A$ is set to 100 nm. Figure 9(a) shows the relation between the bandwidth and the doping concentration of the collect layer after optimization. It can be seen from Fig. 9(a) that the bandwidth increases to flat with the doping concentration lower than $1 \times 10^{16}$ cm$^{-3}$. The doping concentration of $1 \times 10^{16}$ cm$^{-3}$ is chosen to continue optimizing the doping concentration of the cliff layer. As shown in Fig. 9(b), the highest bandwidth of 78.5 GHz can be obtained and the doping concentration of the cliff layer of $1 \times 10^{18}$ cm$^{-3}$ is chosen to determine $W_C$. As illustrated in Fig. 9(c), the bandwidth gets to the peak at $W_C$ = 383 nm and the variation is not more than 4 GHz when $W_C$ is changed from 363 to 413 nm. Then a bandwidth of 83 GHz is obtained according to the above optimization process and more than twice that of the original one. With the device scaling down, the bandwidth can be improved further in our forecast under the sacrifice of response efficiency.

## 5. Conclusions

The performance of the UTC-PD has been investigated by analyzing the impact of the primary parameters on AC performances, which are the most important for a device. The HD model is utilized to analyze the characteristics of the device, and with the analysis, two modified structures are investigated to enhance the bandwidth of the device, with linear doping and linear band-gap method. An optimized device is proposed, increasing the original bandwidth from 38 to 83 GHz.

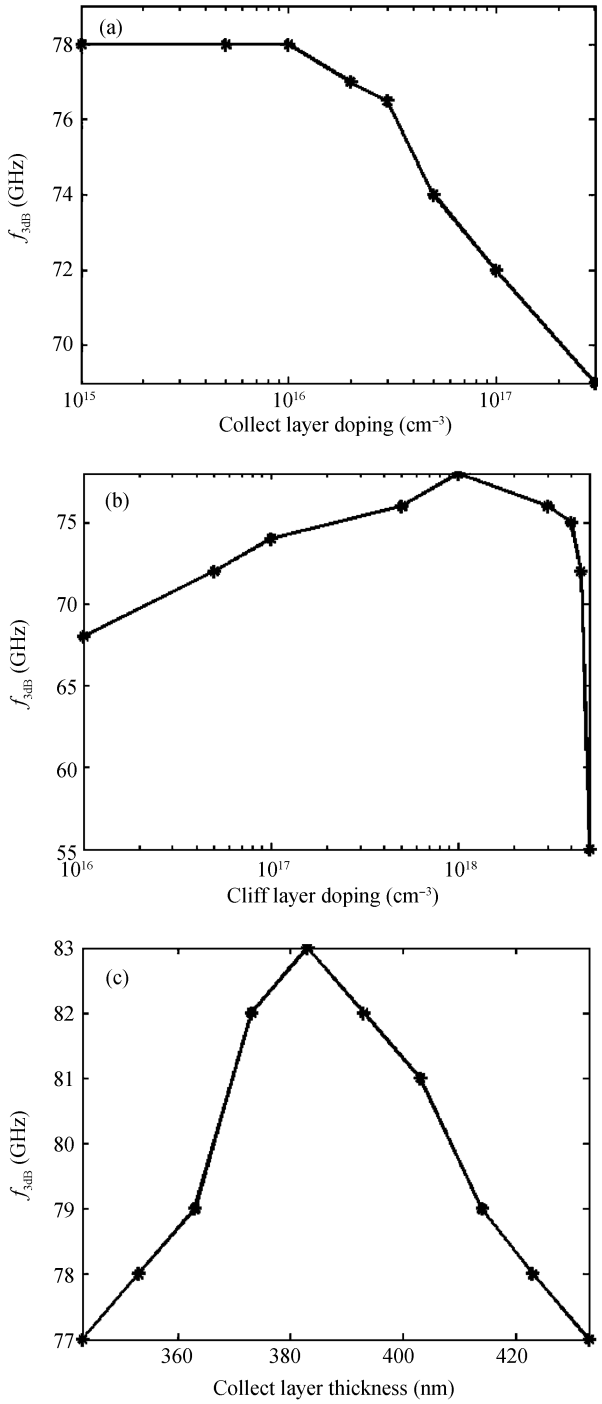


Fig. 9. $f_{3dB}$ versus (a) collection layer doping (using the optimization method and $W_A$ = 100 nm), (b) cliff layer doping (based on the previous step), (c) collect layer thickness (based on the previous step).

## References

[1] Ishibashi T, Kodama S, Shimizu N, et al. High-speed response of uni-traveling-carrier photodiodes. Jpn J Appl Phys, 1997, 36: 6263

[2] Ito H, Furuta T, Kodama S, et al. InP/InGaAs uni-traveling-carrier photodiode with 220 GHz bandwidth. Electron Lett, 1999, 35(18): 1556

[3] Ito H, Kodama S, Muramoto Y, et al. High-speed and high output InP–InGaAs unitraveling-carrier photodiodes. IEEE J Sel Topics Quantum Electron, 2004, 10(4): 709

[4] Beling A, Pan H, Chen H, et al. Measurement and modeling of a high-linearity modified uni-traveling carrier photodiode. IEEE Photonics Technol Lett, 2008, 20(14): 1219

[5] Ito H, Turuta T, Kodama S, et al. InP/InGaAs uni-travelling-carrier photodiode with 310 GHz bandwidth. Electron Lett, 2000, 36(21): 1809

[6] Shi J W, Wu Y S, Lin Y S. Near-ballistic uni-traveling-carrier photodiode based V-band optoelectronic mixers with internal up-

conversion-gain, wide modulation bandwidth, and very high operation current performance. IEEE Photonics Technol Lett, 2008, 20(11): 939

[7] Banik B, Vukusic J, Hjelmgren H, et al. Optimization of the UTC-PD epitaxy for photomixing at 340 GHz. Int J Infrared Milli Waves, 2008, 29(10): 914

[8] Rahman S M M, Hjelmgen H, Vukusic J, et al. Hydrodynamic simulations of unitraveling-carrier photodiodes. IEEE J Quantum Electron, 2007, 43(11): 1088

[9] Ishibashi T, Furuta T, Fushimi H, et al. InP/InGaAs uni-traveling-carrier photodiodes. IEICE Trans Electron, 2000, E83-C(6): 938

[10] Li Xiaojian, Zhang Yejin, Li Guoyu, et al. An equivalent circuit model for uni-traveling-carrier photodiode. Journal of China Universities of Posts and Telecommunications, 2009, 16(1): 40

[11] Banik B, Vukusic J, Hjelmgren H, et al. Optimization of the UTC-PD epitaxy for photomixing at 340 GHz. Int J Infrared Milli Waves, 2008, 29(10): 914

[12] Gonzalez B, Palankovski V, Kosina H, et al. An energy relaxation time model for device simulation. Solid-State Electron, 1999, 43(9): 1791

[13] Inc. Synopsys, Taurus_device, Version 2004.09

[14] Shimizu N, Watanabe N, Furuta T, et al. Electron diffusivity in p-InGaAs determined from the pulse response of InP/InGaAs uni-traveling-carrier photodiodes. Appl Phys Lett, 2000, 76(9): 1191